LOCAL DENSITY OF STATES CALCULATIONS FOR PHOTONIC CRYSTALS

Timothy N. Langtry
Department of Mathematical Sciences
University of Technology, Sydney
NSW 2007, Australia
e-mail: Tim.Langtry@uts.edu.au

Lindsay C. Botten
Department of Mathematical Sciences
University of Technology, Sydney
NSW 2007, Australia
e-mail: Lindsay.Botten@.uts.edu.au

Ara A. Asatryan
School of Physics
University of Sydney
NSW 2006, Australia
e-mail: ara@physics.usyd.edu.au

Ross C. McPhedran
School of Physics
University of Sydney
NSW 2006, Australia
e-mail: r.mcphedran@physics.usyd.edu.au

Abstract

Photonic crystals are a novel class of optical materials that, almost certainly, will underpin major advances in future communication and computer technology. In a photonic crystal, the periodic distribution of refractive index gives rise to interferometric action which leads to band gaps, or frequency ranges for which light cannot propagate. Material or structural defects in the crystal can give rise to localised states, or field modes, that are the analogues of impurity modes in semiconductors, changing the radiation dynamics of the crystal and providing the ability to mould the flow of light in a variety of ways. The radiation dynamics are characterised by the local density of states (LDOS) and, in this paper, we describe a new, highly accurate and efficient technique based on field multipole methods for computing the LDOS. Its implementation on SMP systems using the OpenMP and MPI protocols is discussed and we illustrate its applicability in studies of ordered and disordered crystals. The latter are of particular significance as they provide a framework for investigating fabrication tolerances for realistic crystals.

Key words and phrases

Photonic crystals, Monte Carlo, MPI, OpenMP

1 INTRODUCTION

Photonic crystals (Soukoulis, 1995; Joannopoulos, Meade and Winn, 1999) are a novel type of material in which the refractive index varies periodically with position and which prohibit

the propagation of electromagnetic waves for some frequencies, giving rise to "band gaps" in their spectrum. Photonic crystals have the capacity to "tailor" the flow of light, and thus represent a key approach to the design of components for future integrated photonics (Fan and Joannopoulos, 2000; Noda, Chutinan and Imada 2000; Parker and Charlton, 2000).

Initially, much theoretical and experimental research was carried out to calculate band diagrams and find the transmission and reflection spectra of such structures (Soukoulis, 1995), but this gives little insight into their radiation dynamics. However, both pioneering papers in the area (Yablonovitch, 1987; John, 1987) were concerned with changing the density of states, and thus the radiation dynamics of photonic crystals. The key quantity that determines the radiation dynamics of a fluorescent source embedded in a photonic crystal is the spatially resolved, or *local density of states* (LDOS) (Sprik, van Tiggelen and Lagendijk, 1996). In three dimensions, the LDOS provides the spectral distribution of modes to which a fluorescent source couples: if, for a particular frequency, the LDOS is large, then this indicates that the light emission at that frequency is enhanced by the structure; correspondingly, a small value of the LDOS indicates suppression of light emission at that frequency. To date, the LDOS has been computed for 1D infinite structures, and for 3D structures of infinite size at isolated points within the unit cell as a function of wavelengths. In both cases, the infinite extent of the structure implies that the LDOS vanishes identically with a band gap, yielding no insight whatsoever about the radiation dynamics of structures of a finite size.

In this paper, we describe the development (§2) of a novel theoretical model, based on the theory of multipole expansions, and the associated computational implementation (§§3–4) on an SGI Origin SMP system. Multipole methods, also known as Rayleigh methods, date back to the classic, 1892 work of Lord Rayleigh (Rayleigh, 1892) who originally developed the technique in the context of electrostatics. However, only since the mid-1970s has the computational potential of the technique, in addition to its analytic application, been recognised. The method has been extended to solve dynamic (i.e. wave) problems in electromagnetics and is a standard tool within our group which has pioneered its application within this context.

While much of the computational modelling in this field employs general purpose Fourier (or plane wave) methods, they can suffer from serious convergence difficulties and an inability to model finite (i.e. realistic) systems. The source of these convergence problems is two-fold through (a) the series representation of discontinuous functions (which are particularly severe for high index contrasts) and (b) the intrinsic disadvantage of using a global basis to model structures with a wide variation of scale size. In contrast, the multipole method (McPhedran, Botten, Asatryan, Nicorovici, Robinson and de Sterke, 1999; Botten, Nicorovici, McPhedran, Asatryan, Robinson and de Sterke, 2000; Asatryan, Robinson, Botten, McPhedran, Nicorovici and de Sterke, 1999; Asatryan, Busch, McPhedran, Botten, de Sterke and Nicorovici, 2001) is based on local, multipole field expansions about each scatterer that explicitly satisfy boundary conditions and which yield highly accurate and computationally efficient solutions. The method is applicable to both finite and infinite periodic systems and, unlike the plane wave method, generates exact solutions, yielding a most useful tool through which to gain insight and understanding of the underlying physical processes in realistic systems. Its structure is also amenable to implementation on parallel computer systems.

While the treatment of §2 is for 2D structures and a 2D source, it is readily generalised to a

point source, and further 3D scattering geometries. Finally, §5 shows some applications of relevance to the design of key components of future photonic devices.

2 THEORETICAL FORMULATION

The LDOS $\rho(\mathbf{r};\omega)$ follows from the imaginary part of the trace of the electric Green tensor $\mathbf{G}^e(\mathbf{r},\mathbf{c}_s;\omega)$ that is the solution of the field problem at a point $\mathbf{r}$, for a cluster of N_c cylinders of radii $\{a_l\}$ and refractive indices $\{n_l\}$, due to a line source located at $\mathbf{c}_s$ at a frequency ω:

$$\rho(\mathbf{r};\omega) = -\frac{2\omega}{\pi c^2}\mathrm{Im}\mathrm{Tr}[\mathbf{G}^e(\mathbf{r},\mathbf{r};\omega)]. \tag{1}$$

For simplicity and brevity, we outline only the treatment for $E_{\shortparallel}$ polarised light for which the electric field vector is aligned with the cylinder axes (the $z-$axis). In this case, the only non-trivial component of $\mathbf{G}_e$ is $V^e \stackrel{\text{def}}{=} G^e_{zz}$ that satisfies the boundary value problem

$$\nabla^2 V^e(\mathbf{r};\mathbf{c}_s) + k^2 n^2(\mathbf{r}) V^e(\mathbf{r};\mathbf{c}_s) = \delta(\mathbf{r}-\mathbf{c}_s), \tag{2}$$

where V^e and $\nu \cdot \nabla V^e$ are continuous across all cylinder boundaries. Here, $k = \omega/c$ is the free-space wavenumber, $n(\mathbf{r})$ denotes the refractive index of the cylinders or the background matrix, and ν is the outward normal unit vector to the surface of the cylinders.

In the vicinity of each cylinder l, the exterior field in the matrix of refractive index $n_b = 1$ is expanded in local coordinates $\mathbf{r}_l = (r_l, \theta_l) = \mathbf{r} - \mathbf{c}_l$,

$$V^e(\mathbf{r};\mathbf{c}_s) = \sum_{m=-\infty}^{\infty} \left[A^l_m J_m(kr_l) + B^l_m H^{(1)}_m(kr_l)\right] e^{im\theta_l}, \tag{3}$$

and involves both singular or irregular components characterised by coefficients B^l_m and regular components characterised by A^l_m. This expansion is valid only in the annulus extending from the surface of the cylinder l to the surface of the nearest cylinder or source.

A global field representation, known as the Wijngaard expansion, valid everywhere in the matrix may be derived (for example, see Asatryan, Busch et al., 2001) using Green's theorem:

$$V^e(\mathbf{r};\mathbf{c}_s) = \chi^{\text{ext}}(\mathbf{c}_s) H^{(1)}_0(k|\mathbf{r}-\mathbf{c}_s|)/(4i) + \sum_{q=1}^{N_c}\sum_{m=-\infty}^{\infty} B^q_m H^{(1)}_m(k|\mathbf{r}-\mathbf{c}_q|) e^{im\arg(\mathbf{r}-\mathbf{c}_q)}. \tag{4}$$

Here, the first term is due to the inhomogeneous source term in (2) (with $\chi^{\text{ext}}(\mathbf{c}_s)$ acting as a source term switch), while the second is associated with scattered radiation sourced by each of the cylinders q.

Equating the global (4) and the local (3) forms of the field expansions in the vicinity of cylinder l, and applying Graf's addition theorem to the global form in order to change the field phase origin to the centre of cylinder l, we derive the Rayleigh multipole field identity

$$A^l_m = K^l_m + \sum_{q=1, q\neq l}^{N_c}\sum_{p=-\infty}^{\infty} S^{lq}_{mp} B^q_p. \tag{5}$$

Equation (5) indicates that the regular part of the local field in the vicinity of cylinder l is due to a combination of (a) the exterior source (which, when expanded in a local expansion, is characterized by coefficients K_m^l), and (b) sources on all other cylinders ($q \neq l$), the contributions of which to the multipole term of order $m-p$ at cylinder l is given by S_{mp}^{lq}. The particular forms of the S_{mp}^{lq} and K_m^l and details of the derivation may be found in Asatryan, Robinson et al. (2000). The field identity is most conveniently cast in matrix form

$$\mathbf{A} = \mathbf{SB} + \mathbf{K} \tag{6}$$

and typifies the form arising in all problems solved using the Rayleigh multipole method. Here, $\mathbf{A} = \left[\mathbf{A}^l\right]$, $\mathbf{B} = \left[\mathbf{B}^l\right]$ and $\mathbf{K} = \left[\mathbf{K}^l\right]$ denote partitioned vectors and $\mathbf{S} = \left[\mathbf{S}^{lq}\right]$ denotes a partitioned matrix. As is explained in §3, this form is particularly amenable to implementation on parallel systems.

The coefficients $\mathbf{A}$ and $\mathbf{B}$ are linked by the boundary conditions, viz. the continuity of the tangential components of the electric and magnetic fields across cylinder-matrix interfaces. We begin with a local expansion of the field interior to cylinder l,

$$V^e(\mathbf{r};\mathbf{c}_s) = \sum_{m=-\infty}^{\infty} Q_m^l H_m^{(1)}(kn_l r_l)e^{im\theta_l} + \sum_{m=-\infty}^{\infty} C_m^l J_m(kn_l r_l)e^{im\theta_l}, \tag{7}$$

in which the first series on the right hand side denotes a possible, interior field source

$$\chi_l^{\text{int}}(\mathbf{c}_s)H_0^{(1)}(kn_l|\mathbf{r}-\mathbf{c}_s|)/(4i),$$

analogous to the exterior source in (4). The boundary conditions are then readily expressed in the form

$$\mathbf{B} = \mathbf{RA} + \mathbf{TQ}, \tag{8}$$

$$\mathbf{C} = \mathbf{T}'\mathbf{A} + \mathbf{R}'\mathbf{Q}, \tag{9}$$

where the matrices $\mathbf{R}$, $\mathbf{T}$, $\mathbf{R}'$ and $\mathbf{T}'$ are block diagonal matrices containing diagonal blocks representing cylindrical harmonic reflection and transmission coefficients. In (8) and (9), the regular exterior field $\mathbf{A}$ and the irregular interior field $\mathbf{Q}$ are regarded as "incoming" fields, generating the irregular exterior $\mathbf{B}$ and regular interior $\mathbf{C}$ fields.

The Rayleigh identity, in the form of a system of linear equations in the source coefficients $\mathbf{B}$, is then deduced from (6) and (8) yielding

$$(\mathbf{I}-\mathbf{RS})\mathbf{B} = \mathbf{RK} + \mathbf{TQ}, \tag{10}$$

in which the right hand side represents the reflection of a source $\mathbf{K}$ exterior to the cylinder or the transmission of an interior source $\mathbf{Q}$ through cylinder interfaces. By solving the partitioned system of linear equations (10), the multipole coefficients $\mathbf{B}^l$ are determined and the Green function can be reconstructed from its exterior (4) and interior (7) Wijngaard expansions.

3 COMPUTATIONAL METHODS

To gain insight into the radiation dynamics of a photonic crystal it is necessary to compute the LDOS at a set of points in the crystal. The set may comprise a single point, or may

sample the entire structure, yielding an LDOS map of the crystal. The computational problem in this case is to develop a code which is both efficient and sufficiently flexible to be applicable across this range. For convenience, we consider source points lying on a uniform rectangular grid Z containing $N_{\mathbf{r}} = N_x \times N_y$ points:

$$Z = \{(x_0 + i_x \delta x, y_0 + i_y \delta y) : i_x = 0, \ldots, N_x - 1; i_y = 0, \ldots, N_y - 1\}.$$

Here δx and δy denote the mesh increments, and for convenience of notation we take the corresponding value to be 1 in the case that $N_x = 1$ or $N_y = 1$.

Of particular significance are the effects on the radiation dynamics of perturbations in the material and geometric properties, yielding insight into the tolerances acceptable in the manufacture of photonic crystals. In particular, we are interested in how sensitive the LDOS is to random perturbations in the positions of the scattering cylinders, their radii, and their refractive indices. A corresponding computational problem is to estimate the mean LDOS corresponding to random perturbations of these quantities with specified distributions.

We consider first the case of a single, unperturbed crystal. As mentioned in §2, equation (10) is representative of the structure of multipole methods. Of particular importance is the fact that the coefficient matrix $(\mathbf{I} - \mathbf{RS})$ depends only on the optical and geometrical properties of the array of scatterers—it is independent of the source term, dependence on which is restricted to the right hand side term $\mathbf{RK} + \mathbf{TQ}$. Consequently we use a single *LU* factorisation of the coefficient matrix to solve (10) for the coefficient vector $\mathbf{B}$ corresponding to each point of interest in the structure. The computation of each element of the coefficient matrix requires multiple Bessel function evaluations and consequently the initialisation of the matrix requires substantial execution time. Nevertheless, this time can be reduced by exploiting the loop-level parallelism inherent in the problem—we use OpenMP (Chandra, Dagum, Kohr, Maydan, McDonald and Menon, 2001) in a shared memory environment to populate the coefficient matrix in parallel threads. Similarly, the solution of the linear system for each source point in the map requires multiple Bessel function evaluations within a sum. Again we can exploit loop level parallelism using OpenMP, with a reduction operation to accumulate the required sum. The *LU* factorisation of the coefficient matrix is performed by the relevant LAPACK routine (Anderson et al., 1999).

Next we consider the study of the effects of random perturbations of the crystal structure. We use a Monte Carlo simulation to estimate the mean LDOS corresponding to perturbations with given distributions. In particular, we apply a sequence of pseudo-random perturbations to a given crystal structure, yielding a sample set of crystal instances. Each instance is then analysed by the code described above. Since individual instances have little data in common, these analyses can be executed by separate processes in a distributed environment, although each process utilises shared memory parallelism as described above. The resulting simulation program is structured using a master-slave strategy, with the MPI library (Pacheco, 1997) being used to implement the required message passing. The master process is responsible for generating the sequence of crystal instances. Each instance is then passed to a slave process which generates the corresponding LDOS map using OpenMP and returns it to the master. The master process is then responsible for accumulating the ensemble average LDOS and tracking the convergence of the process.

Convergence is treated heuristically by tracking the change, between successive instances, in the squared sample mean, normalised to the size of the map. In particular, let $\epsilon = (\epsilon_{\mathbf{r}}, \epsilon_{\mathbf{a}}, \epsilon_{\mathbf{n}})$

be a partitioned vector denoting a random perturbation of the positions, radii and refractive indices of the cylinders comprising the crystal. Denote by $\rho(\mathbf{r}, \epsilon; \omega)$ the LDOS of the perturbed crystal, by $\overline{\rho}(\mathbf{r}, \omega)$ the mean LDOS at $\mathbf{r}$ and ω of the perturbed crystals, and define the ensemble average of a sample of N_I perturbations by $\widehat{\rho}_{(N_I)}(\mathbf{r}; \omega) \stackrel{\text{def}}{=} \frac{1}{N_I} \sum_{j=1}^{N_I} \rho(\mathbf{r}, \epsilon; \omega)$. We estimate the absolute error $\|\overline{\rho}(\cdot; \omega) - \widehat{\rho}_{(N_I)}(\cdot; \omega))\|_2 = \left[\int \left(\overline{\rho}(\mathbf{r}; \omega) - \widehat{\rho}_{(N_I)}(\mathbf{r}; \omega)\right)\right)^2 d\mathbf{r}\Big]^{1/2}$ by

$$\delta_{\widehat{\rho}}(N_I) \stackrel{\text{def}}{=} \sqrt{\sum_{\mathbf{r} \in Z} \left(\widehat{\rho}_{(N_I)}(\mathbf{r}; \omega) - \widehat{\rho}_{(N_I - 1)}(\mathbf{r}; \omega)\right)^2 \delta\mathbf{r}},$$

where $\delta\mathbf{r} = \delta x \delta y$. A corresponding estimate of the relative error is then easily obtained. We note that, although a rectangular grid is used to obtain the LDOS maps presented in this paper, the method can also be applied with non-uniform grids. These are of advantage where the LDOS varies rapidly in certain regions but not in others.

4 PERFORMANCE

Table 1 reports the wall time, total cpu time and percentage of cpu usage (cpu%) for the program in the case of analysing a single instance of a 2D photonic crystal comprising 136 cylinders. The crystal is described in greater detail in §5—here we are concerned with the performance of the program. The code was run in four different configurations, each with one master process and one slave process, the latter using 1, 2, 4 or 8 threads. We observe from Table 1 that total cpu time tends to diminish as the number of threads increases: this is due to the fact that for most of the time the master process is idling while waiting for the slave to complete its analysis. Consequently, since the wall time (and hence the wasted master process cpu time) decreases with an increasing number of threads, the total cpu time also tends to decrease. The exception is for 4 threads, where the total cpu time exceeds that required for 2 threads. We attribute this to the fact that the SGI Origin system on which the code was run, whilst a shared memory machine, has non-uniform memory access times. In particular, as more cpus are used, both the likelihood of, and costs associated with, non-near memory accesses increase.

Use of the program for the analysis of a single crystal instance is inherently inefficient because of the master/slave dichotomy, even though the master requires just one processor to the slave's k_t (one for each thread). On the other hand, Table 2 reports the performance of the

Table 1: Performance data for analysis of a single 2D photonic crystal of 136 cylinders. Configuration: 1 master process plus 1 slave, with the slave having k_t threads.

k_t	Wall time *h:m:s*	Total cpu time *h:m:s*	cpu%
1	2:45:40	5:30:13	200
2	1:25:00	4:13:40	305
4	0:52:20	4:19:32	500
8	0:26:20	3:54:33	902

program for a set of 40 realisations of 2D crystals, each again comprising 136 cylinders. As described in §5, these realisations may be thought of as modelling small deviations from a given design during manufacture. Timing data is reported for a range of configurations: master plus k_s slaves ($k_s = 1, \ldots, 4$), with each slave having either $k_t = 4$ or $k_t = 8$ threads. Total cpu time varies across the listed configurations by 19.8% of the lowest cpu time. The code's performance appears to scale well with the number of slaves, although again we observe that, comparing the results for 4 and 8 threads per slave, total cpu time is consistently lower for $k_t = 4$ than for $k_t = 8$.

Table 2: Performance data for analysis of a set of 40 two-dimensional photonic crystals of 136 cylinders. Configuration: 1 master process plus k_s slaves, with each slave having k_t threads.

k_s	k_t	Wall time *h:m:s*	Total cpu time *h:m:s*	cpu%
1	4	34:03:56	167:56:26	533
1	8	19:53:51	171:30:14	963
2	4	16:00:40	143:20:50	975
2	8	9:29:00	157:07:03	1705
3	4	11:47:20	149:38:06	1312
3	8	6:31:20	155:54:38	2495
4	4	8:43:40	143:09:26	1699
4	8	5:30:40	160:00:13	3284

5 APPLICATION

The LDOS is a measure of the extent to which the environment can control the properties of an emitter such as an atom. Indeed, spontaneous emission by an atom or molecule whose transition lies in a band gap is suppressed as there are no available states into which emission can occur. The key to the operation of a photonic crystal is their appearance as an ideal, lossless mirror when operated in a band gap—with obvious implications for use in lasing (as the containment mechanism) and guided signal propagation. Highly advantageous effects can be obtained if perfect periodicity is violated. This is best exploited in photonic band gap (PBG) materials, where structural or material defects give rise to localized modes (analogous to the impurity modes of semiconductors) that appear in the band gap to form defect states through which emission may occur (Yablonovitch, 1987). For photonic crystals containing photoactive media, the material may emit light over a wide spectral range, but only those wavelengths matching the defect states can propagate out of the crystal. This is important in developing microlasers and LEDs with the number and size of the defects controlling the spectral width and threshold. Similarly, the removal of entire lines or planes of scatterers produces a band of defect states that enable the channel to guide light. PBG guiding is both lossless and efficient as there are no states that let light leak from the guide, normally an overwhelming problem.

As an example we model a waveguide obtained by cutting a channel through a rectangular

Figure 1: Plots of $\log_{10} \rho(\mathbf{r}; \omega)$ along a cross-section (lying on the y axis) of a photonic crystal (a) without the waveguide channel, and (b) with the waveguide channel. Both plots indicate exponential decay of the LDOS with increasing distance into the bulk of the crystal. Plot (b) indicates also a range of frequencies at which the LDOS remains high in the waveguide while having low values in the remainder of the crystal. Plots (c) and (d) indicate the corresponding crystal structures by giving a view down the vertical axis, parallel to the cylinders.

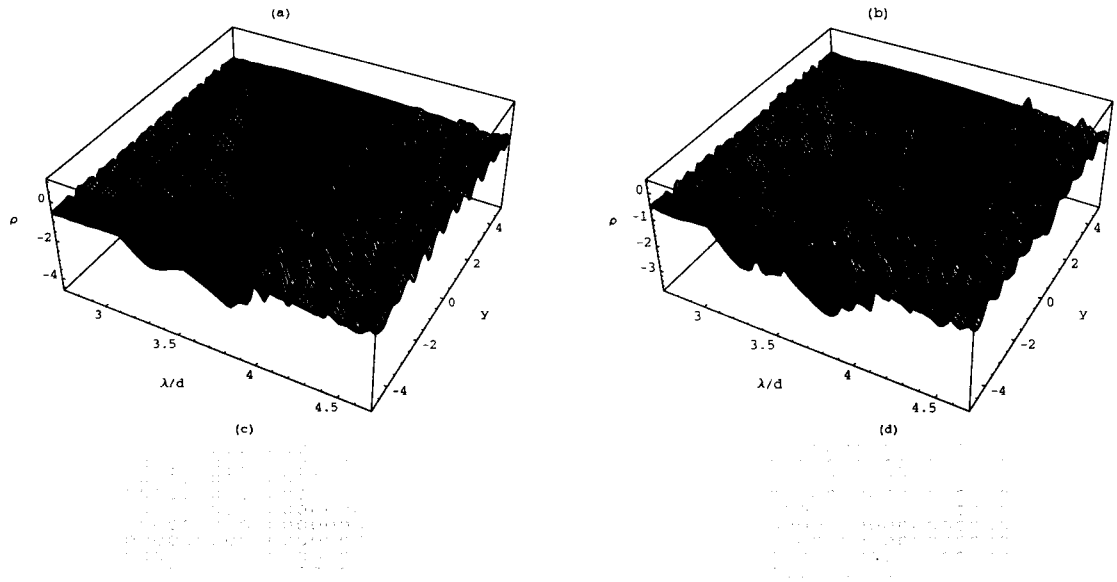

array of cylinders (Mekis, Chen, Kurland, Fan, Villeneuve and Joannopoulos, 1996) whose centres are separated by a distance of d units in the direction of each coordinate axis. In the following discussion, the optical properties of the material are assumed to be dispersionless (i.e., independent of wavelength) and all wavelengths λ are normalised to the period of the structure (i.e., λ/d). The cylinders are all of normalised radius $a_l/d = 0.3$ units and their refractive indices are all $n_l = 3$.

We consider first the ideal, finite structure without the channel. The corresponding infinite structure exhibits a photonic band gap that manifests itself as an LDOS of precisely 0. In the case of the finite structure, the LDOS is strongly reduced for frequencies in the gap, but is not precisely zero, and indeed, for larger crystals, the LDOS at a fixed point inside the structure decays exponentially as the size of the crystal increases. At other frequencies light propagates readily. Figure 1 illustrates the existence of a band gap by plotting the logarithm of the LDOS ρ against frequency along a cross-section ($x = 0$) of the crystal, both in the complete structure (Fig. 1a) and in the waveguide structure (Fig. 1b).

As an example, in Figure 2 we see that for $\lambda/d = 3.3$ the LDOS within the guide is high relative to its value in the bulk crystal and slightly enhanced relative to its free space value. Also evident is the efficient channeling of light around a sharp bend without significant radiation losses. In contrast, conventional dielectric waveguides (such as optical fibres) are unable to efficiently transmit light through tight, or intricate, paths without substantial bending losses.

Figure 2: Surface and contour plots of ρ for a photonic crystal with channel. The LDOS is plotted for $\lambda/d = 3.3$, a normalised frequency at which the crystal demonstrates strong guiding properties.

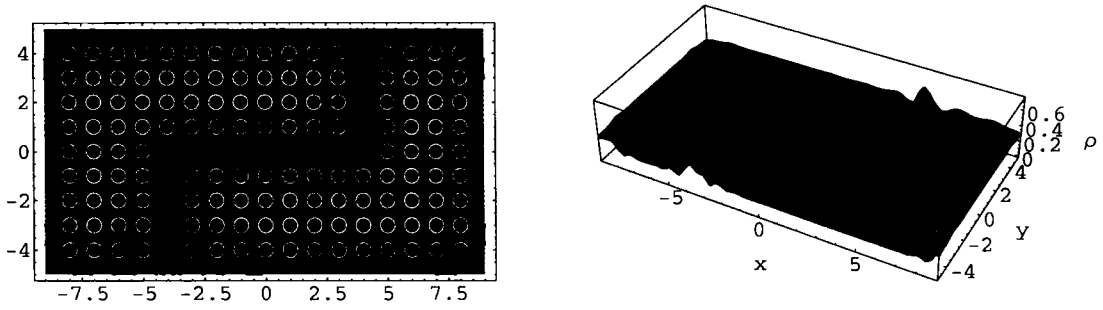

While photonic crystal waveguides can efficiently guide light, particularly around sharp bends, little is known about the effect on signal propagation of scattering losses arising from fabrication defects. We thus consider the sensitivity of the LDOS to perturbations of the waveguide structure. In particular, we consider:

(a) random perturbations, uniformly distributed on (i) $[-0.03, 0.03]$ and (ii) $[-0.1, 0.1]$, of the radius of each cylinder,

(b) random perturbations, uniformly distributed on (i) $[-0.3, 0.3]$ and (ii) $[-1.0, 1.0]$, of the refractive index of each cylinder.

These trials may be interpreted as representing random variations, of maximum 10% in case (i) and $33\frac{1}{3}\%$ in case (ii), from an ideal crystal . The ensemble averages $\widehat{\rho}_{40}^{(a)}$ and $\widehat{\rho}_{40}^{(b)}$ of ρ over a set of 40 perturbed instances were computed independently for cases (a) and (b) respectively, and are plotted in Figure 3. In case (i) it is clear that the crystals still, on average, demonstrate substantial guiding properties. However, at the $33\frac{1}{3}\%$ level [case (ii)], the mean LDOS indicates that these properties have been lost. Figure 4 plots the value of the convergence indicators $\delta_{\widehat{\rho}}(N_I)$ for case (ii).

We conclude with the simulation of the random laser, a major, recent advance in the field (Cao, Xu, Zhang, Chang, Ho, Seelig, Liu and Chang, 2000). Here, the cylinders of the photonic crystal are composed of material with gain and the structure is disordered, giving rise to field localisation—that is, exponential decay of the field arising from the strong scattering caused by the extreme disorder of the structure (John, 1984). Provided that the field containment (due to localisation) is sufficiently strong and that the amplification is sufficiently high, laser action can occur. In Fig. 5 we see traces of the formation of closed loops at the lower left edge of the cluster where the amplification of light appears as an enhancement of the Green's function due to a source located in the centre of the cluster.

Figure 3: Contour plots of the ensemble averages $\widehat{\rho}_{40}^{(a)}$ and $\widehat{\rho}_{40}^{(b)}$ for crystals with perturbed radii (left) and refractive indices (right).

Case (i): random variations with maximum deviation 10% from the ideal design of the crystal.

(a) (b)

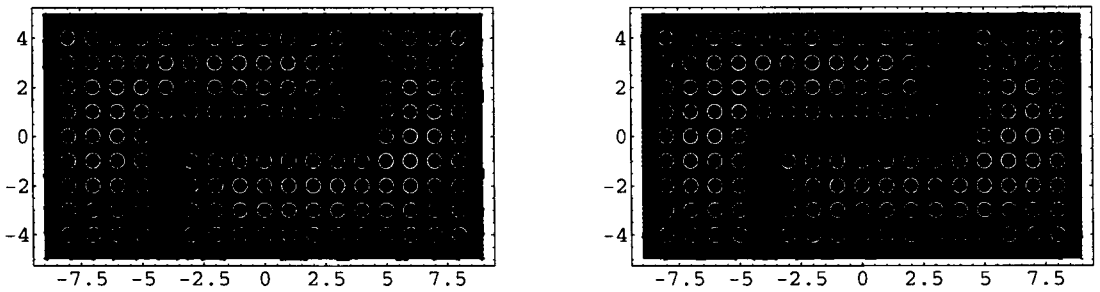

Case (ii): random variations with maximum deviation $33\frac{1}{3}\%$ from the ideal design of the crystal.

(a) (b)

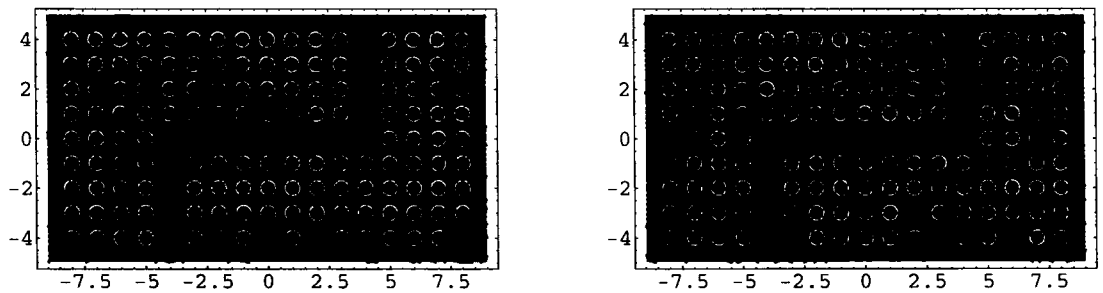

Figure 4: Convergence of ensemble averages for perturbed (a) radii and (b) refractive indices in case (ii): perturbations were uniformly distributed with a $33\frac{1}{3}\%$ maximum deviation from the mean value.

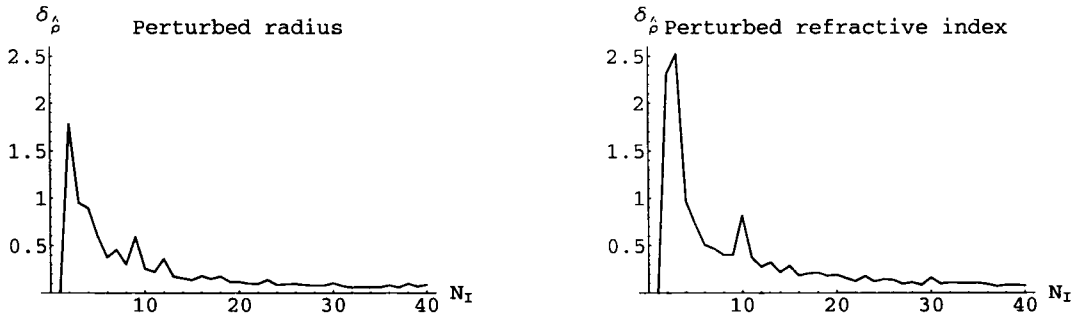

Figure 5: A strongly disordered photonic crystal composed of material with gain.

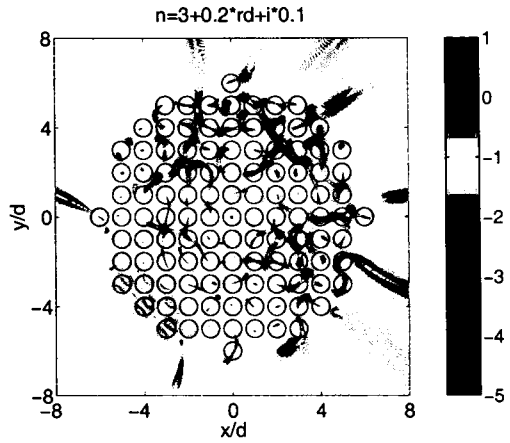

References

[1] ANDERSON, E., BAI, Z., BISCHOF, C., BLACKFORD, S., DEMMEL, J., DONGARRA, J., DU CROZ, J., GREENBAUM, A., HAMMARLING, S., MCKENNEY, A. and SORENSON, D. (1999): LAPACK Users' Guide (3rd edn). Philadelphia, SIAM.

[2] ASATRYAN, A. A., BUSCH, K., MCPHEDRAN, R. C., BOTTEN, L. C., DE STERKE, C. M. and NICOROVICI, N. A. (2001). Phys. Rev. E 63:046612.

[3] ASATRYAN, A. A., ROBINSON, P. A., BOTTEN, L. C., MCPHEDRAN, R. C., NICOROVICI, N. A. and DE STERKE, C. M. (1999). Phys. Rev. E 60:6118.

[4] ASATRYAN, A. A., ROBINSON, P. A., BOTTEN, L. C., MCPHEDRAN, R. C., NICOROVICI, N. A. and DE STERKE, C. M. (2000). Phys. Rev. E 62:5711.

[5] BOTTEN, L. C., NICOROVICI, N. A., MCPHEDRAN, R. C., ASATRYAN, A. A., ROBINSON, P. A. and DE STERKE, C. M. (2000). J. Opt. Soc. Am. A, 17:2169.

[6] CAO, H., XU, J. Y., ZHANG, D. Z., CHANG, S.-H., HO, S. T., SEELIG, E. W., LIU, X. and CHANG, R. P. H. (2000). Phys. Rev. Lett. 84:5584.

[7] CHANDRA, R., DAGUM, L., KOHR, D., MAYDAN, D., MCDONALD, J. and MENON, R. (2001): Parallel Programming in OpenMP. San Diego, Academic Press.

[8] FAN, S. and JOANNOPOULOS, J. D. (2000): Optics & Photonic News 11(10):28. See also the site http://ab-initio.mit.edu/photons/micropolis.html.

[9] JOANNOPOULOS, J. D., MEADE, R. D. and WINN, J. N. (1995): Photonic Crystals: Molding the Flow of Light. Princeton University, New Jersey. See also the special issue on photonic crystals in: Journal of Lightwave Technology (1999), 17(11).

[10] JOHN, S. (1984). Phys. Rev. Lett. 53:2169.

[11] JOHN, S. (1987). Phys. Rev. Lett. 58:2486.

[12] MCPHEDRAN, R. C., BOTTEN, L. C., ASATRYAN, A. A., NICOROVICI, N. A., ROBINSON, P. A. and DE STERKE, C. M. (1999). Aust. J. Phys., 52:791.

[13] MEKIS, A., CHEN, J. C., KURLAND, I., FAN, S., VILLENEUVE, P. R. and JOANNOPOLULOS, J. D. (1996). Phys. Rev. Lett. 77:3787.

[14] NODA, S. N., CHUTINAN, A. C. and IMADA, M. (2000). Nature 407:608.

[15] PACHECO, P. (1997): Parallel Programming with MPI. San Francisco, USA, Morgan Kaufman.

[16] PARKER, G. and CHARLTON, M.(2000). Physics World 8:29.

[17] RAYLEIGH, LORD, (1892). Philos. Mag. 34:481.

[18] SOUKOULIS, C. M., (Edit.) (1995): Photonic Band Gap Materials. NATO Series vol. 315, Dordrecht, Netherlands, Kluwer.

[19] SPRIK, R., VAN TIGGELEN, B. A. and LAGENDIJK, A. (1996). Europhys. Lett. 35:265.

[20] YABLONOVITCH, E. (1987). Phys. Rev. Lett. 58:2059.

Acknowledgements

The authors would like to acknowledge the support of the Australian Research Council and the Australian Centre for Advanced Computing and Communications (ac3).